JOURNAL OF AIRCRAFT
Vol. 31, No. 5, Sept.–Oct. 1994

Interpretation of Waverider Performance Data Using Computational Fluid Dynamics

Charles E. Cockrell Jr.*
NASA Langley Research Center, Hampton, Virginia 23681

A computational study was conducted to better understand experimental results obtained from wind-tunnel tests of a Mach 4 conical-flow-derived waverider and a comparative reference configuration, which showed that the aerodynamic performance of the reference configuration was slightly better than that of the waverider. The computational results showed that the predicted surface pressure values and the integrated lift and drag coefficients were much lower for the reference model because the reference model bottom is an expansion surface. However, the lift-drag ratios for the reference model were higher due to a relatively low drag for a comparable amount of lift. The results also showed that the reference model exhibited the same shock attachment characteristics as the conical-flow-derived waverider, and is therefore also a waverider. The shock attachment characteristic gives the waverider a performance advantage over conventional hypersonic vehicles, and the results suggest that altering the bottom surface does not cause significant performance degradation. Flowfield solutions also show that the conical-flow waverider model has better propulsion/airframe integration characteristics than the reference configuration. The results also suggest that generating flowfields other than conical ones may be used to design waveriders with improved aerodynamic performance.

Nomenclature

C_D = drag coefficient
C_L = lift coefficient
I, J, K = computational grid axes
M = Mach number
P = static pressure, lbf/ft^2
P_{base} = base pressure, lbf/ft^2
S = planform area, ft^2
V = total volume, ft^3
V_{eff} = volumetric efficiency, $V^{2/3}/S_{ref}$
X, Y, Z = coordinate axis system, in.
y^+ = inner law variable
α = angle of attack, deg

Subscript
∞ = freestream conditions

Introduction

WAVERIDERS are candidate shapes for various types of hypersonic aircraft designs. A waverider is a shape designed from any known supersonic or hypersonic flowfield, such as flow past a right circular cone.[1] The waverider is designed such that the bow shock is attached along the outer leading edge at the design point. A typical waverider design from a conical flowfield is shown in Fig. 1. The leading edge is defined on the conical shock wave and the lower surface is designed by using the known flowfield to trace streamlines from the leading edge to the base of the configuration, resulting in a constant stream surface behind the conical shock wave. A waverider is uniquely defined by a leading-edge definition and a specific set of freestream conditions. The upper surface may be designed as a freestream surface, as a slight expansion surface or by other techniques. The shape is generally optimized for some figure of merit, such as maximum lift-drag ratio or minimum drag at the design point, depending on the application of interest. The attached bow shock creates an efficient compression lifting surface with no flow spillage from the lower surface to the upper surface at the design point. Because of this characteristic, the predicted lift-drag ratios of waveriders are higher than those for conventional hypersonic vehicle concepts.[1] Another advantage of axisymmetric waverider flowfields is that the uniformity of the bottom surface flowfield and the absence of crossflow make the waverider an ideal candidate for scramjet propulsion-system integration.[2]

Previous criticisms of waveriders have been resolved in recent studies,[1,3,4] leading to renewed interest in their use for various hypersonic vehicle designs. One criticism is that early design techniques used only inviscid methods that produced shapes with large surface areas resulting in large skin-friction drag. The lift-drag ratios obtained experimentally were poor compared to predictions. Current design codes include an estimate for skin-friction drag in the optimization process.[1] This improvement allows the optimization routine to minimize wetted surface area and provide more accurate estimates for aerodynamic performance. The class of vehicles designed using this method is called viscous-optimized waveriders. A second concern associated with waveriders is that their off-design performance may be poor, even though on-design performance is excellent. However, recent experimental and computational studies have shown that waveriders that

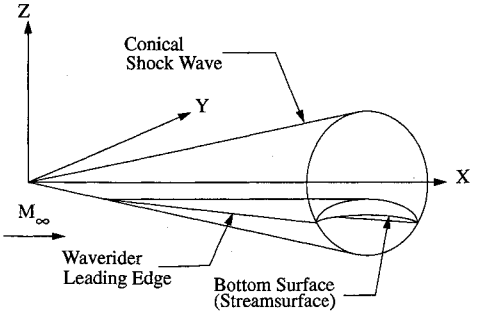

Fig. 1 Waverider designed from conical flowfield.

Presented as Paper 93-2921 at the AIAA 24th Fluid Mechanics Conference, Orlando, FL, July 6–9, 1993; received Oct. 3, 1993; revision received Feb. 2, 1994; accepted for publication Feb. 2, 1994.

*Aerospace Engineer, Hypersonic Airbreathing Propulsion Branch, Gas Dynamics Division, M/S 413. Member AIAA.

demonstrate acceptable off-design performance can be designed.[3,4] Additionally, optimization routines can include various volumetric constraints that allow for the design of shapes with improved volumetric efficiencies and packaging characteristics while accepting a minimum penalty in aerodynamic performance. Previous computational studies have validated design methods and predicted waverider flowfield properties accurately.[4]

Because of the leading-edge shock attachment, resulting from the design method, waveriders have been shown to provide better aerodynamic performance than more classical aerodynamic shapes. A previous experimental study showed that a reference configuration, designed by modifying an optimized conical-flow-derived waverider, provided better aerodynamic performance than the optimized waverider model itself at its design Mach number.[3] Based on prior experience, it was not expected that the modified shape would provide comparable or better aerodynamic performance. It is important to determine the nature of this performance advantage since the interest in waverider-derived vehicle concepts is generated primarily by the high lift-drag ratios produced by waverider flowfields. The purpose of the present study is to interpret these experimental results using computational fluid dynamics (CFD) solutions.

First, this article will present a description of the two configurations studied as well as the elements of the experimental program and a brief description of the results obtained. Next, the computational method will then be presented followed by a discussion of the computational results. Finally, a discussion of how the CFD predictions were used to interpret and explain the experimental data will be presented.

Configuration Design

The two configurations examined in this study were a Mach 4.0 viscous-optimized waverider model and a reference flat-top model of the same planform shape. The waverider model was designed using a waverider design code developed at the University of Maryland.[1,5] This code uses an inviscid design method, but includes an estimate for skin friction in the optimization process, using the integral boundary-layer method. The code also uses a simplex optimization algorithm to optimize shapes for maximum lift-drag ratio or minimum drag at the design point.[5] In this study, the waverider model was optimized for maximum lift-drag ratio at Mach 4.0. Maximum lift-drag ratio is more appropriate as a hypersonic cruise performance parameter than minimum drag. The design point of Mach 4.0 was chosen based on experimental facility limitations and the desire to obtain data at, above, and below the design point, even though the application would be in the hypersonic speed regime. The design freestream Reynolds number was 2.0×10^6/ft, and the model length was 30 in. with a 24-in. span. The top surface was designed as an expansion surface using the axisymmetric method of characteristics in order to provide an additional contribution to lift.

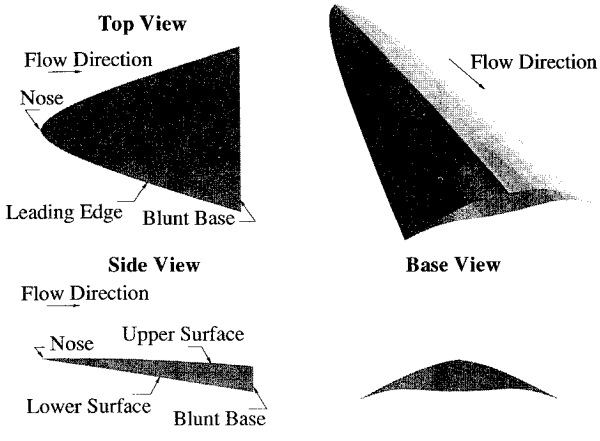

Fig. 2 Mach 4.0 waverider model.

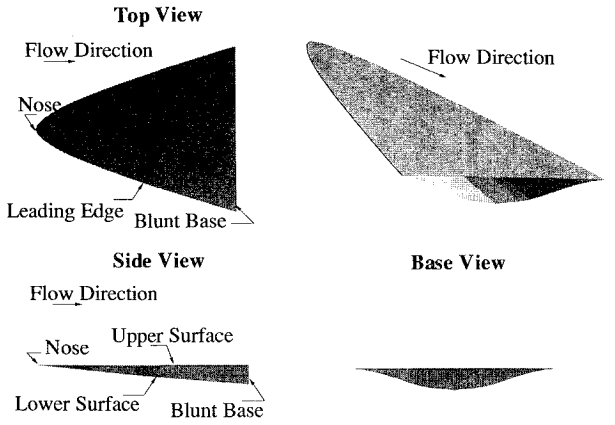

Fig. 3 Flat-top reference model.

Some volumetric constraints were also incorporated into the optimization routine in order to increase volumetric efficiency, from that of the unconstrained shape, and to generate a shape that had good structural characteristics for a wind-tunnel model. Therefore, the maximum lift-drag ratio of the waverider shape studied here is slightly less than that for the unconstrained shape that could be obtained at these freestream conditions. An oblique view and a 3-view sketch of the waverider model is shown in Fig. 2.

A reference flat-top model was designed in order to illustrate the benefits of waverider flowfield properties by comparing the optimized waverider configuration with a shape that has similar characteristics. The flat-top model was designed by adjusting the top surface coordinate of the waverider at each cross section to create a flat surface and then adjusting the corresponding bottom surface coordinate at that cross section by the same increment. The result is a modified waverider configuration with the same thickness at each location and the same planform shape and total volume as the optimized waverider model. Therefore, the volumetric efficiencies are also equal. An oblique view and 3-view sketch of the reference model is shown in Fig. 3.

Experimental Program

An experimental program was conducted in order to investigate the aerodynamic performance of the waverider and reference configurations.[3] Both models were tested in the Unitary Plan Wind Tunnel (UPWT) at NASA Langley Research Center. The configurations were tested over an angle-of-attack range from -16 to 14 deg at Mach 4.0 and at selected off-design Mach numbers in the range of Mach 2.3–4.63 at zero angle of attack. The freestream Reynolds number in each case is 2.0×10^6/ft, which is the nominal operating condition in the UPWT.

Figure 4 shows the experimental values for lift-drag ratio plotted vs lift coefficient for both the waverider and flat-top models at Mach 4.0. For small values of lift, the flat-top model has a higher lift-drag ratio for a given value of lift coefficient. The flat-top configuration also has a higher maximum lift-drag ratio than the waverider model. These data suggest that a modified waverider configuration provides better aerodynamic performance than an optimized conical-flow waverider model at the waverider design Mach number.

Computational Study

In order to interpret the experimental results, a computational study was conducted. The study consisted of obtaining viscous solutions for both configurations using the General Aerodynamic Simulation Program (GASP), version 2.0.[6] GASP version 2.0 can solve the full Reynolds-averaged Navier-Stokes equations as well as subsets of these equations, including the thin-layer Navier-Stokes (TLNS), parabolized Navier-Stokes (PNS), and Euler equations. The solutions shown in this study were obtained by solving the TLNS equations in the nose

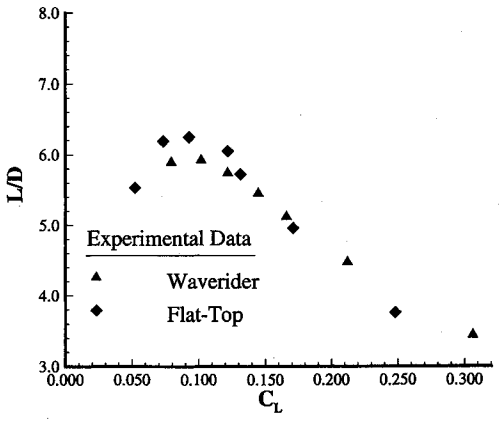

Fig. 4 Experimental values of lift/drag ratio vs C_L for waverider and flat-top models at Mach 4.0 and $Re_\infty = 2.0 \times 10^6$/ft.

region in order to capture the region of subsonic flow behind the detached bow shock and the PNS equations over the remaining configuration. Solutions were obtained for the waverider and flat-top configurations over an angle-of-attack range from 0 to 10 deg at Mach 4.0. Off-design solutions at Mach 3.5 and 4.5 at 0-deg angle of attack were obtained for the waverider only.

The numerical method in GASP is based on the upwind/relaxation algorithms. Time integration is based on the integration of primitive variables and uses a 2-factor approximate factorization scheme. Convergence to a steady-state solution was accomplished by reducing the L2 norm of the residual by 4 orders of magnitude. Van Leer's flux-vector splitting algorithm was used with the exception that full flux is enforced in the marching direction for PNS solutions. Mesh sequencing was used to accelerate convergence for the TLNS solutions. A no-slip boundary condition with a fixed wall temperature of 585°R was imposed on solid boundaries.

The grid used for the waverider solutions was generated from a previous computational study which examined this configuration at the design Mach number only.[7,8] The grid was generated using an algebraic transfinite interpolation method and used an adaptive approach to cluster grid cells in the region of shock waves at the design point. The grid that was adapted for flow at Mach 4.0 and an angle of attack of 0 deg is used for all of the solutions in this study. The waverider grid consisted of 53 points in the streamwise I direction, 71 points in the circumferential J direction, and 51 points in the vertical K direction. The grid for the flat-top geometry was generated using algebraic transfinite interpolation methods with elliptic interior point refinement.[9] The flat-top grid contained 51 points in the streamwise I direction, 71 points in the circumferential J direction, and 61 points in the vertical K direction. Both grids had points clustered near the solid boundaries in order to adequately resolve boundary layers in viscous solutions. The amount of clustering required is determined by examining the inner law variable y^+. Previous studies have shown that y^+ values on the order of 1.0 will yield an accurate solution.[10] Additionally, both grids modeled the blunt leading edges of the wind-tunnel models. Grid points are clustered around the leading edge in the circumferential direction in order to adequately resolve the flowfield in this region.

Lift and drag coefficients were obtained by integrating pressures predicted by CFD solutions over the configuration surfaces. An estimate for skin friction is included in the computational lift and drag values using the reference temperature method[11] in order to make some limited comparisons with experimental data. All experimental and computational data presented are corrected for base drag by assuming freestream pressure acting at the base. The blunt base of the configuration will be eliminated by the addition of control surfaces and a propulsive nozzle in any practical waverider-based configuration. Therefore, it is necessary to eliminate base drag from the results. It is also important to consider the method of base pressure correction since the method used can have a significant effect on the relative performance of two configurations.[12] The method of assuming freestream pressure acting at the base is consistent with the approach used in the design code.

Results

The results from the computational study are presented in two parts. First, lift and drag coefficients from waverider integrated surface pressure predictions are presented as a function of Mach number. Second, flowfield solutions as well as lift and drag coefficients from integrated surface pressure predictions are presented for both the flat-top model and the waverider at Mach 4.0 and various angles of attack. Comparisons of surface pressure predictions and performance characteristics of each configuration are made. Comparisons between experimental data and CFD predictions are presented in some cases.

Lift and drag coefficients for the waverider model at 0-deg angle of attack for the design Mach number of 4.0 and for

Table 1 Lift and drag coefficients from integrated surface pressure predictions for waverider model for Mach 4.0 and off-design Mach numbers at 0-deg angle of attack

M_∞	C_L	C_D	Lift/drag ratio
3.5	0.0823	0.0121	6.80
4.0	0.0747	0.0144	6.47
4.5	0.0677	0.0106	6.39

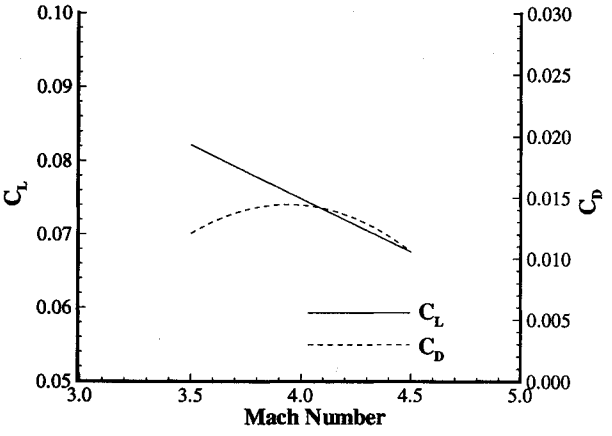

Fig. 5 CFD predictions with skin friction estimate for C_L and C_D vs Mach number for waverider model.

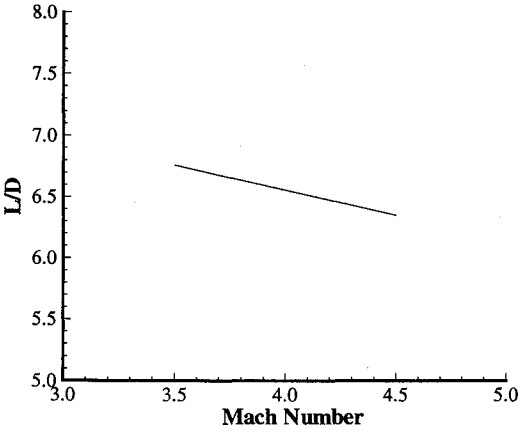

Fig. 6 CFD predictions with skin friction estimate for lift/drag ratio vs Mach number for waverider model.

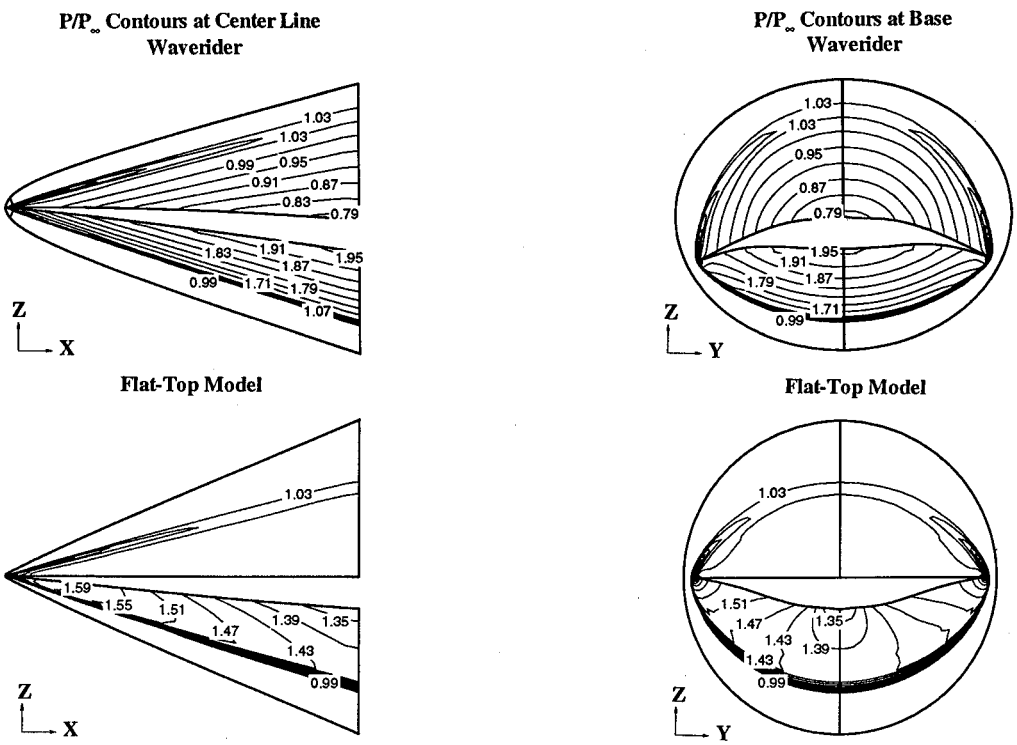

Fig. 7 CFD flowfield solutions of waverider and flat-top models at Mach 4.0, $Re_\infty = 2.0 \times 10^6$/ft and $\alpha = 0$ deg.

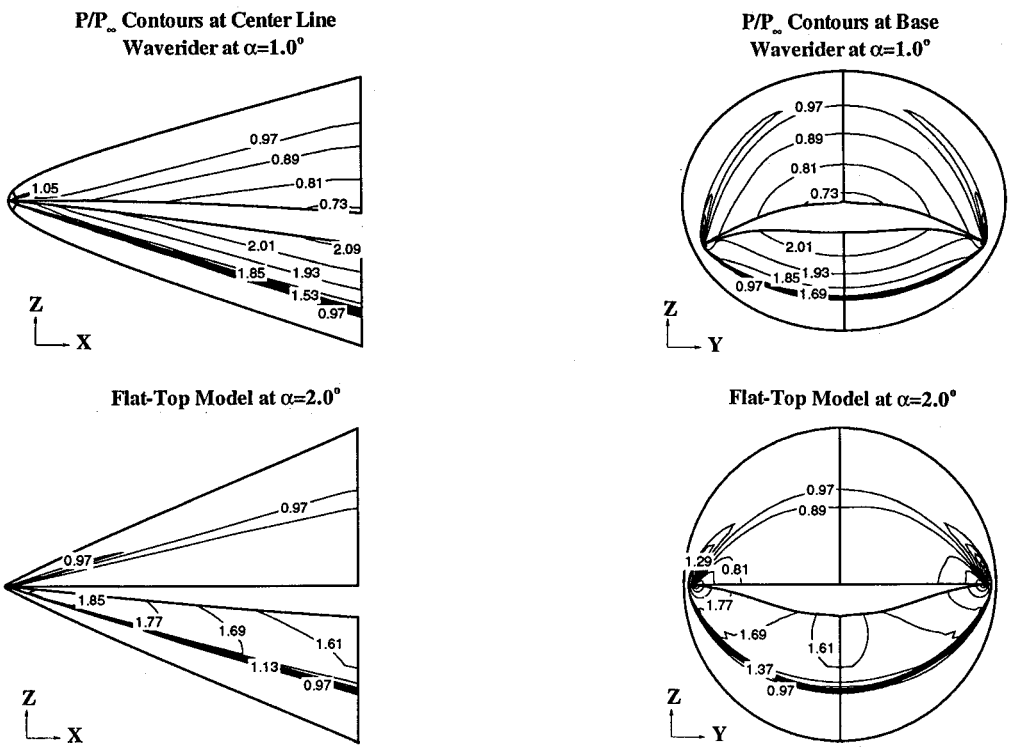

Fig. 8 CFD flowfield solutions of waverider and flat-top models at Mach 4.0, $Re_\infty = 2.0 \times 10^6$/ft and maximum lift/drag ratio condition for each model ($\alpha = 1$ deg for waverider, $\alpha = 2$ deg for flat-top model).

off-design Mach numbers are shown in Table 1. The predictions for lift coefficient, drag coefficient, and lift-drag ratio are shown in Figs. 5 and 6, respectively. These results indicate that lift decreases as Mach number increases and freestream Reynolds number per foot remains constant. The drag has a maximum value at Mach 4.0 and the lift-drag ratio decreases with increasing Mach number. This result is also consistent with Ref. 3, which showed that the performance of waveriders does not degrade significantly at off-design conditions.

A comparison of the waverider and reference configuration flowfields shows some of the differences between the two models. Figure 7 shows solutions of the waverider and flat-top configurations at Mach 4.0 and 0-deg angle of attack. Static pressure contours are shown for the centerline and the base of each model. The most notable difference is that the bottom-surface pressure values are considerably lower for the flat-top configuration than for the waverider model. An examination of the geometry reveals that the bottom surface of the flat-top configuration has a slight expansion, due to the method that was used to design this configuration. In contrast, the bottom surface of the waverider model is a compression surface. The solutions at the base of each model show that

the shock is slightly detached for each configuration. This detachment is due to boundary-layer displacement and blunt leading-edge effects. Since the design code assumes an infinitely sharp leading edge and uses an inviscid approach with only an estimate for skin friction used to calculate force coefficient predictions, the shock is detached slightly from the leading edge of the model even at the design point. The high-pressure region is still mostly confined to the bottom surface. The flat-top model exhibits the same shock attachment properties as the waverider model because it has the same projected planform shape as the waverider, and both models have adequately shallow initial compression angles in the streamwise plane. The base view of the waverider shows that this configuration has a uniform, conical flowfield behind the shock wave. The flat-top model does not exhibit this property.

Solutions are shown in Fig. 8 for the condition where maximum lift-drag ratio is observed to occur for each configuration at the design Mach number. Static pressure contours are shown at the centerline and base of the waverider model at 1-deg angle of attack and the reference model at 2-deg angle of attack. The bottom surface pressure values for the flat-top model are still lower than those for the waverider. The flat-top model still exhibits the same waverider shock attachment properties although the shock detachment distance increases as angle of attack increases. The bottom surface of the flat-top model does not show the highly uniform conical flowfield that the waverider does. This is the property that makes the conical-flow-derived waverider an ideal candidate for scramjet integration. Therefore, the reference configuration does not have good propulsion/airframe integration (PAI) characteristics, even though it shows slightly better aerodynamic performance than the conical-flow-derived waverider.

The lower pressure values on the bottom surface of the flat-top configuration correspond to lower lift and drag values. The lift and drag coefficients from integrated surface pressure predictions for the waverider and flat-top models at Mach 4.0 are shown in Tables 2 and 3, respectively. At all angles of attack studied, the predicted values of both lift and drag coefficients are lower for the flat-top model than for the waverider. The aerodynamic performance characteristics of each configuration are examined by presenting the lift and drag predictions as a function of angle of attack and the lift-drag ratios as a function of lift coefficient.

Table 2 Lift and drag coefficients from integrated surface pressure predictions for waverider model at Mach 4.0 and selected angles of attack

α	C_L	C_D	Lift/drag ratio
0.0	0.0747	0.0115	6.45
1.0	0.0934	0.0144	6.47
2.0	0.1139	0.0190	5.99
3.0	0.1283	0.0233	5.56
4.0	0.1558	0.0290	5.37
6.0	0.2204	0.0480	4.59
10.0	0.3168	0.0909	3.39

Table 3 Lift and drag coefficients from integrated surface pressure predictions for flat-top model at Mach 4.0 and selected angles of attack

α	C_L	C_D	Lift/drag ratio
0.0	0.0476	0.0081	5.87
1.0	0.0617	0.0092	6.74
2.0	0.0807	0.0118	6.82
3.0	0.0996	0.0152	6.53
4.0	0.1183	0.0194	6.11
6.0	0.1692	0.0325	5.20
10.0	0.2487	0.0644	3.86

The predicted and experimental lift and drag characteristics, together with CFD predictions, of each configuration at various angles of attack are shown in Figs. 9 and 10 for the design Mach number of 4.0. The variation of lift coefficient with angle of attack is presented in Fig. 9. This figure shows that the lift coefficient values for the waverider model are higher than those for the flat-top model at each angle of attack. These results are expected based on the predicted pressure values in the computational solutions. Good agreement is generally obtained between the CFD solutions and the experimental values. The drag coefficient data are presented in Fig. 10. In both cases, higher drag values are shown

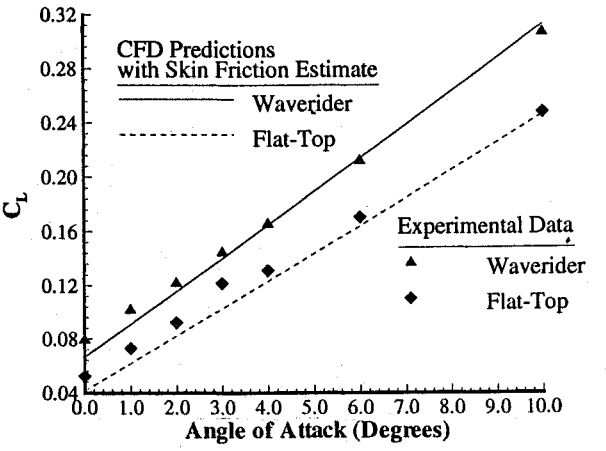

Fig. 9 CFD predictions and experimental values of C_L vs α for waverider and flat-top models at Mach 4.0 and $Re_\infty = 2.0 \times 10^6$/ft.

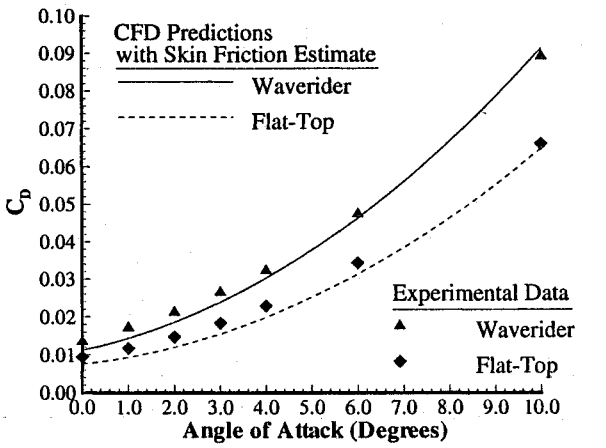

Fig. 10 CFD predictions and experimental values of C_D for waverider and flat-top models vs α at Mach 4.0 and $Re_\infty = 2.0 \times 10^6$/ft.

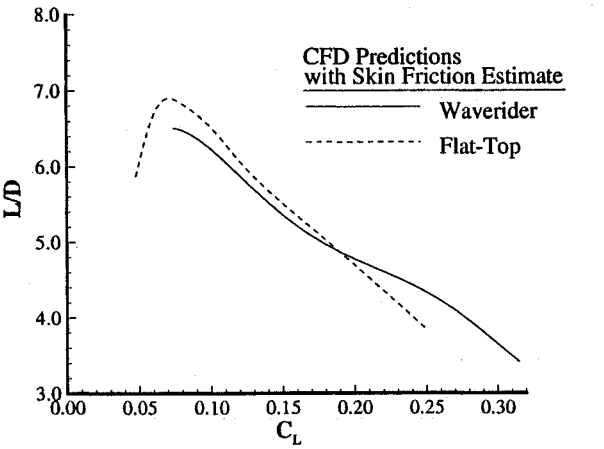

Fig. 11 CFD predictions of lift/drag ratio vs C_L for waverider and flat-top models at Mach 4.0 and $Re_\infty = 2.0 \times 10^6$/ft.

for the waverider model at each angle of attack. The drag values for the waverider also increase more rapidly as the angle of attack increases. Again, good agreement is generally obtained between CFD results and experimental data.

The lift-drag ratio as a function of lift coefficient is presented in Fig. 11. For small values of lift, the flat-top model has a higher lift-drag ratio than the waverider. These results also show that the flat-top model has a higher maximum lift-drag ratio, but at a smaller value of lift coefficient. The CFD predictions for performance agree with the experimental results and the CFD flowfield solutions provide an indication of why these results were observed.

Interpretations

Several interpretations can be made by comparing computational solutions of both configurations with each other and by comparing computational predictions of both configurations with experimental data. The waverider configuration has higher lift than the reference flat-top configuration for all conditions investigated. However, the flat-top model has a higher lift-drag ratio at some points and a higher maximum lift-drag ratio than the waverider model due to relatively lower drag. In other words, for small values of lift, the drag coefficient is lower for the flat-top model than for the waverider, due to the lower bottom-surface pressures. This results in a higher lift-drag ratio for the flat-top model at most conditions. The bottom surface of the flat-top model has a slight expansion and therefore, lower surface pressure.

The flat-top model exhibits the same shock attachment properties as the waverider model because they both have adequately shallow initial compression angles. The projected planform shape of the reference model is also identical to that of the waverider model, which has a leading edge defined on the conical shock wave. Based on the improved performance of the flat-top model, it can be concluded that the basic physical effect that gives the waverider its advantage in aerodynamic performance over conventional hypersonic vehicles is the shock attachment caused by the streamwise shape of the leading edge. Therefore, even though the flat-top model is not a conical-flow-derived waverider, it still has the basic characteristic that gives waveriders an advantage in aerodynamic performance, and is therefore also a waverider. The design code utilized in this study cannot generate this shape in the optimization routine because it is not a conical-flow derived waverider. However, the flat-top configuration does not possess good PAI characteristics because it does not have the uniform conical flowfield present in the waverider flowfield, even though it shows higher maximum lift-drag ratios than the waverider at small values of lift. Moreover, the results suggest that the bottom surface of a waverider can be altered somewhat without a significant degradation in aerodynamic performance. This implies that altering the bottom surface of a waverider configuration to integrate engine components should not degrade the performance of the vehicle significantly as long as the planform shape is maintained. Since the reference configuration has been shown to be a nonconical-flow-derived waverider, the results further suggest that different generating flowfields may be used to design waveriders that have better aerodynamic performance than conical-flow-derived waveriders.

Conclusions

A computational study was conducted to better understand the results obtained from an experimental investigation of a Mach 4 conical-flow-derived waverider and a reference flat-top configuration. The results from this experiment showed that the flat-top configuration had a higher maximum lift-drag ratio than the waverider model. The waverider model was designed using an optimization routine that includes an estimate for skin friction in the optimization process. The reference model was designed by adjusting the top surface of the waverider to obtain a flat surface, while maintaining the same planform shape and thickness at each location.

Viscous solutions were obtained for both configurations, and lift and drag predictions were obtained from these solutions by integrating surface pressure values and including an estimate for skin friction. Solutions of the waverider at the design Mach number and selected off-design Mach numbers showed that the off-design performance of the waverider does not degrade significantly at off-design conditions. The bottom-surface pressures of both the waverider and flat-top model at Mach 4.0 and selected angles of attack showed that the bottom surface of the flat-top model provides a slight expansion, in contrast to the waverider bottom surface, which acts as a compression surface. The result is that the lift and drag predictions for the flat-top model are much lower than those for the waverider model. These characteristics result in higher lift-drag ratios for the flat-top model at smaller values of lift. However, the differences in performance between the two configurations are primarily due to the shape of the bottom surface, which results in a lower lift coefficient value at the maximum lift-drag ratio condition for the flat-top model.

The CFD results also show that the reference configuration exhibits the same shock attachment properties as the waverider. The results from this study suggest that the leading-edge shock attachment is the main effect that gives waveriders their high lift-drag ratios. However, even though the flat-top model provides higher lift-drag ratios at lower values of lift, it does not have the uniform bottom surface flowfield that makes the waverider a good candidate for scramjet propulsion-system integration. Both characteristics, as well as other considerations, are important in the development of any practical waverider-based vehicle. The results further suggest that other generating flowfields may be used to generate waveriders with improved aerodynamic performance over conical-flow-derived waveriders.

References

[1]Bowcutt, K. G., and Anderson, J. D., "Viscous Optimized Hypersonic Waveriders," AIAA Paper 87-0272, Jan. 1987.

[2]O'Neill, M. K., and Lewis, M. J., "Optimized Scramjet Integration on a Waverider," *Journal of Aircraft*, Vol. 29, No. 6, 1992, pp. 1114–1121.

[3]Bauer, S. X. S., "Analysis of Two Viscous Optimized Waveriders," First International Hypersonic Waverider Symposium, Univ. of Maryland, College Park, MD, Oct. 1990.

[4]Takashima, N., and Lewis, M. J., "Navier-Stokes Computation of a Viscous-Optimized Waverider," AIAA Paper 92-0305, Jan. 1992.

[5]Corda, S., and Anderson, J. D., "Viscous Optimized Hypersonic Waveriders Designed from Axisymmetric Flow Fields," AIAA Paper 88-0369, Jan. 1988.

[6]McGrory, W. D., Huebner, L. D., Slack, D. C., and Walters, R. W., "Development and Application of GASP 2.0," AIAA Paper 92-5067, Dec. 1992.

[7]Jones, K. D., Bauer, S. X. S., and Dougherty, F. C., "Hypersonic Waverider Analysis: A Comparison of Numerical and Experimental Results," AIAA Paper 91-1696, June 1991.

[8]Jones, K. D., "Numerical Simulation of High-Speed Flows About Waveriders with Sharp Leading Edges," *Journal of Spacecraft and Rockets*, Vol. 29, No. 5, 1992, pp. 661–667.

[9]Steinbrenner, J. P., Chawner, J. R., and Fouts, C. L., "The GRIDGEN 3D Multiple Block Grid Generation System," Flight Dynamics Lab., Wright Research and Development Center, WRDC-TR-90-3022, Wright-Patterson Air Force Base, OH, July 1990.

[10]Richardson, P. F., and Parlette, E. B., "Comparison Between Experimental and Numerical Results for a Research Hypersonic Aircraft," *Journal of Aircraft*, Vol. 27, No. 4, 1990, pp. 300–305.

[11]Sommer, S. C., and Short, B. J., "Free-Flight Measurements of Turbulent-Boundary-Layer Skin Friction in the Presence of Severe Aerodynamic Heating at Mach Numbers from 2.8 to 7.0," NACA TN-3391, March 1955.

[12]Cockrell, C. E., Jr., "Interpretation of Waverider Performance Data Using Computational Fluid Dynamics," AIAA Paper 93-2921, July 1993.